Article

Insight into the Catalytic Performance of a Zinc-Pillared Curcumin/Bentonite Composite for Enhanced Oxidation of Ibuprofen Residuals into Environmental Products: The Pathway and Toxicity

Sarah I. Othman [1], Marwa H. Shemy [2,3], Haifa E. Alfassam [1], Haifa A. Alqhtani [1], Ahmed A. Allam [4,5], Mostafa R. Abukhadra [3,6,*] and Stefano Bellucci [7,*]

[1] Biology Department, College of Science, Princess Nourah bint Abdulrahman University, Riyadh 11671, Saudi Arabia; healfassam@pnu.edu.sa (H.E.A.)
[2] Chemistry Department, Faculty of Science, Beni-Suef University, Beni-Suef 65211, Egypt
[3] Materials Technologies and their Applications Lab, Geology Department, Faculty of Science, Beni-Suef University, Beni-Suef 65211, Egypt
[4] Zoology Department, Faculty of Science, Beni-Suef University, Beni-Suef 65211, Egypt; ahmed.aliahmed@science.bsu.edu.eg
[5] Department of Biology, College of Science, Imam Mohammad Ibn Saud Islamic University (IMSIU), Riyadh 11623, Saudi Arabia
[6] Geology Department, Faculty of Science, Beni-Suef University, Beni-Suef 65211, Egypt
[7] INFN, Laboratori Nazionali di Frascati, E. Fermi 54, 00044 Frascati, Italy
* Correspondence: abukhadra89@science.bsu.edu.eg (M.R.A.); stefano.bellucci@lnf.infn.it (S.B.); Tel.: +20-01288447189 (M.R.A.)

Abstract: Environmental organo bentonite synthesis using curcumin-derived chemicals is used as catalyst support for zinc with a Zn-pillaring structure (Zn@CU/BEN). The obtained composite was assessed as an affordable, highly effective, and multifunctional photocatalyst for enhanced oxidation of ibuprofen (IBU) residuals in water supplies. The Zn@CU/BEN composite (0.4 g/L) displayed significant catalytic activities, resulting in the complete oxidation of IBU (25 mg/L) after 80 min. Then, the complete mineralization based on the full elimination of TOC content was recognized after 160 min, with significant indications about the formed intermediates. The identified intermediates, together with the identification of hydroxyl radicals as the essential oxidizing agent, declared an oxidation pathway of IBU over Zn@CU/BEN that involved three steps: hydroxylation, decarboxylation/demethylation, and ring-opening processes. The toxic properties of raw pollutants as well as the oxidizing product at different durations were assessed based on the cell viability results of kidney (HEK293T) and liver (HepG2) cell lines. The partially oxidized sample in the initial duration displayed a higher toxicity impact than the raw IBU. However, the treated sample after 160 min reflected high biosafety and non-toxic properties (cell viability > 97%). The synergetic impact of bentonite and bentonite organo-modified by curcumin extract reflects enhancements in the adsorption as well as the oxidation performance of pillared zinc as a catalyst.

Keywords: bentonite; curcumin; zinc metal; ibuprofen; oxidation; toxicity

1. Introduction

A broad range of medication residues, together with their metabolic byproducts, have been recorded to have shown up extensively in a variety of natural environments, including sewage water, surface water, groundwater, and drinking water [1,2]. The pollution of vital drinking water supplies with these chemicals correlates with the discharging of waste effluents from hospitals, drug industries, and healthcare institutes in addition to human excrement [1,3]. Ibuprofen (IBU) is a frequently utilized non-steroidal medicine with antipyretic, anti-inflammatory, and analgesic properties. It has been extensively

identified as an organic contaminant or pharmaceutical residue in water bodies [4,5]. IBU possesses an extremely high yearly consumption of approximately 15,000 tons per year and has been described as one of the top 50 medications with the greatest environmental hazards [6,7]. The leftovers of IBU encountered in water bodies were categorized as hazardous, non-biodegradable, and chemically resistant pollutants [5,8]. The presence of IBU, including its metabolic byproducts, within the water resources, regardless of minimal levels, has a detrimental effect on the endocrine system's functioning in humans and the reproductive abilities of aquatic organisms [8–10]. The IBU-soluble molecules exhibit bioaccumulation characteristics in fish and other aquatic life and have adverse influences on existing freshwater plants and animals [11]. Furthermore, the IBU molecules undergo frequent conversion into types of secondary compounds such as 4-isobutylacetophenone, which exist widely within the freshwater supplies and are more hazardous than the original compounds [11]. Moreover, long-term exposure to IBU has detrimental impacts on both human liver cells and kidney cells, regardless of whether the contact is brief [12].

Due to its classification as a hazardous contaminant, significant endeavors have been launched by environmental and scientific organizations to eliminate IBU from water [1,8]. In recent times, the implementation of adsorption alongside advanced oxidation as effective methods for removing organic chemicals from water has been highly promoted [13,14]. Advanced oxidation techniques, including photocatalytic, electrochemical, sonochemical, and photo-Fenton decomposition, were recently classified as highly successful approaches for decontaminating organic compounds [15–17]. The advanced methods of oxidation result in extensive degrading and mineralization of organic compounds, leading to the formation of environmentally safe compounds [18,19]. In this regard, a variety of individual and combined nano/microstructures were evaluated for their capacity to photocatalytically oxidize and photo-Fenton oxidize IBU residues within water [3,9]. Selecting a suitable catalyst to provide promising oxidation effects is determined by several factors, spanning both environmental and commercial aspects, including recycling potential, biodegradability, bandgap energy, recovery, thermal stability, recombination speeds, security, production cost, and efficiency of adsorption [20,21]. With these in mind, it was strongly recommended that efforts should go toward developing inventive structures, employing naturally existing precursors, which exhibit improved adsorption and oxidizing abilities [22].

Several inorganic materials, including semi-conductive metals as well as metal oxides, were explored as possible photocatalysts. These materials were assessed either as pure in nature or blends with other components [22–24]. The latest studies focused on investigating multifunctional materials that exhibit enhanced optical and retention properties, with the goal being to to develop enhanced photocatalysts [9,24]. Zinc-based nano- and microstructures were extensively analyzed as potential photocatalysts to trigger the oxidative decomposition of organic compounds [22,25]. Overall, this material exhibits outstanding properties such as excellent durability, non-toxicity, biocompatibility, a substantial surface area, sufficient resistance against photo-corrosion, and noteworthy oxidation capacities. Additionally, it possesses considerable potential for free excitation energy [26–28]. The utilization of Zn or ZnO as a photocatalyst can be improved by incorporating them into composite materials, supplementing their structures with rare metals, and embedding their particulates inside appropriate carriers. This approach has been suggested as a straightforward method that can improve the photocatalytic effectiveness, including regeneration, recombination rate, exciting effectiveness, and adsorption capacity [22,29].

However, studies that have been conducted in this area reveal notable impacts of factors such as crystal structure, morphological characteristics, synthesizing techniques, mechanical strength, crystallite dimensions, hybridization, and surface-modifying procedures on the qualities and applications of zinc-based materials [26,30,31]. Elsewhere, in research evaluating zinc-based hybrids with various types of biopolymers produced using naturally occurring phytochemicals derived from plant-based extracts led to the production of environmentally friendly products with improved technical characteristics [27,32]. Thus, it seems that when employing solutions extracted from edible plants that are en-

riched in various types of widely recognized phytochemicals, the production of zinc-based nanostructures based on these extracts as a green synthesis method may yield materials with improved physicochemical and environmental characteristics. This approach was highly praised for the development of non-agglomerated nanostructures. The resulting nanoparticles have been identified to have affordable manufacturing costs, require effortless fabrication processes, and boast non-toxicity, a reactive functionalized surface, and safety [27,33]. Additionally, the nanoparticles that were produced were thoroughly coated with films of phytochemicals, including phenolic chemicals, alkaloids, amino acids, and proteins, forming types of metal/phytochemical complexes. These phytochemical coatings enhance the exterior properties of the resulting particles, facilitating the adsorption of organic molecules on their surfaces [27].

Against that background, this work entailed a thorough analysis of the implementation of a bentonite multilayered structure as an efficient substrate or carrier of green-formed Zn metal, curcumin-derived phytochemicals, and complexes of Zn/curcumin-based phytochemicals as an improved environmentally friendly catalytic agent. Curcumin is a naturally occurring pigment with a diphenolic β-diketone structure that is obtained directly from the rhizome of *Curcuma longa* L., frequently referred to as turmeric. It is extensively utilized as a spice and a medicinal ingredient [34]. The extremely symmetrical arrangement of delocalized π electrons within curcumin along with its derived compounds gives rise to remarkable electrical together with optical abilities [34,35]. Recently, it has been established as a photosensitive agent for use in photodynamic treatment, demonstrating antibacterial and anticancer properties. The formulation of a curcumin-based complex containing zinc has already been employed for various environmentally friendly uses, including the elimination of arsenite, fluoranthene, perylene, and chrysene [35]. Curcumin has the ability to reduce the level of organic compounds when paired with metal oxide nanoparticles. Consequently, its combination with zinc oxide might augment its capacity to adsorb and boost its photocatalytic activity [35].

Bentonite (BEN) is a versatile type of clay mineral that is frequently employed in various environmental sectors. It has distinctive characteristics that enable it to be utilized as an adsorbent alongside being a support material for metals and metal-oxide-based catalysts [36–38]. BEN is distinguished by its abundant availability, excessive ion exchange potential, reactive surface, large surface area, non-toxic qualities, biocompatibility, and ability to adsorb and absorb chemicals. These qualities make it a valuable carrier for certain metals, as it assists in enhancing both the physical and chemical characteristics of the catalyst [36,39]. In this study, the incorporation of zinc into the bentonite layers has been accomplished by pillaring the metal together with curcumin, which served as both the reduction and capping reagents. This process resulted in the formation of a zinc-capped curcumin or zinc/curcumin complex as pillared units between the bentonite layers, forming a hybrid structure denoted as Zn@CU/BEN. The incorporation of curcumin-derived phytochemicals proceeded through a conventional organic intercalation procedure, and we utilized its extract to produce a specific type of safe organo-modified bentonite.

The synthetic catalyst was assessed experimentally as a potential and effective photocatalyst for enhanced degradation of IBU residuals from water supplies in the presence of a visible light source. The catalytic activity was monitored based on the degradation percentages in terms of the affected experimental variables, the TOC content and mineralization degree, the formed intermediate compounds and suggested pathway, and the kinetic properties. Moreover, our study involved a detailed toxicological investigation of the treated sample after different oxidation intervals, to follow the toxicity of the intermediate compound and the safety limitations of the applied photocatalytic degradation system of IBU based on the Zn@CU/BEN catalyst.

2. Results and Discussion

2.1. Characterization of the Catalyst

The structural impact of synthesis, including the crystallized phases, was evaluated based on XRD patterns (Figure 1). The employed BEN precursor exhibits the distinctive peaks of montmorillonite (5.78° (001) as well as 6.95° (002)), which are its primary constituents, together with specific impurities like kaolinite and quartz (ref. card no. 000-003-0010) (Figure 1A). The estimated crystallite size and d-spacing values of the montmorillonite component are 12.9 nm and 12.71 Å, respectively. The acid treatment of BEN caused significant modifications with respect to the crystalline structure of montmorillonite. The key peaks exhibited a significant shift towards lower levels (5.05° and 6.6°), accompanied by a notable decrease in their magnitudes (Figure 1B). These reflect the partially destroying effect of the acid on the BEN lattice structure, which is often accompanied by improvements in the reactivity, textural properties, and physicochemical behaviors of the modified product [40,41]. The XRD pattern of Zn@CU/BEN confirmed the different integration and modification steps, including the intercalation of the curcumin-related organic phytochemicals and the Zn-pillaring step (Line c in Figure 1). The intercalation step resulted in a marked exfoliation impact on the bentonite layered units, which was reflected in the notable amorphization or destruction of its structure and the significant intensification of the d-spacing to 26.3 Å (Line c in Figure 1). The intercalated curcumin was confirmed by three corresponding detectable peaks at 12.2°, 14.42°, and 19.5° (Line c in Figure 1). Also, the pillaring of Zn metals with 10.8 nm crystallite size was confirmed by the reduced peaks within the area from 30° to 80° (36.41° (002), 39.0° (100), 43.30° (101), 54.41° (102), and 36.40° (101)) (Figure 1B) (JCPDS 36–1451; JCPDS 00-004-0784).
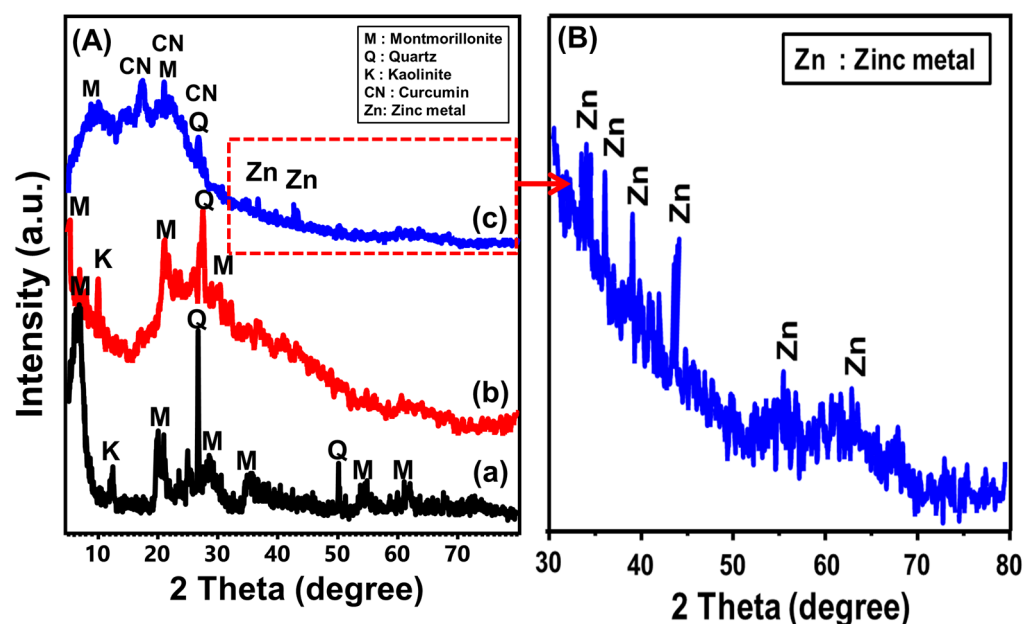

Figure 1. (**A**) XRD patterns of the synthetic structures (raw BEN (a), activated BEN (b), and synthesized Zn@CU/BEN (c)) and (**B**) focus view on the diffraction peaks of zinc metal.

Concerning morphology, the employed bentonite substrate could be distinguished as having prominent aggregation consisting of packed and compressed flake-like particulates (Figure 2A). The distinct cornflake shape of montmorillonite was readily apparent in the high-resolution photos, where the montmorillonite platelets displayed bent and curved shapes (Figure 2B). The HRTEM photo of BEN particulates exhibited an obvious and substantial multilayered interior framework, showcasing the distinctive lattice figures typical of montmorillonite (Figure 2C). Following the addition of curcumin-derived extract, the layered units of BEN expanded and separated notably (Figure 2D). The HRTEM photos also revealed the interplay of the clay sheets with tiny coatings of polymeric organic

molecules, which could potentially be associated with the derived chemical from curcumin (Figure 2). The filamentous forms were clearly visible and had a darker gray color relative to the silicate sheets of BEN (Figure 2E). The synthesized Zn@CU/BEN particulates had highly decorative exfoliated layers that were capped with many spherically shaped granules of the synthesized pillared zinc metal (Figure 2F). The development and dispersion of the aforementioned pillared metallic zinc nanoparticles frequently resulted in interconnecting nanopores, which had a substantial beneficial impact on the surface area (Figure 2G,H). The HRTEM scans revealed an array of synthesized zinc nanoparticles distributed inside the BEN layers, confirming their development as pillared nanostructures and surficial-coated sheets (Figure 2I).
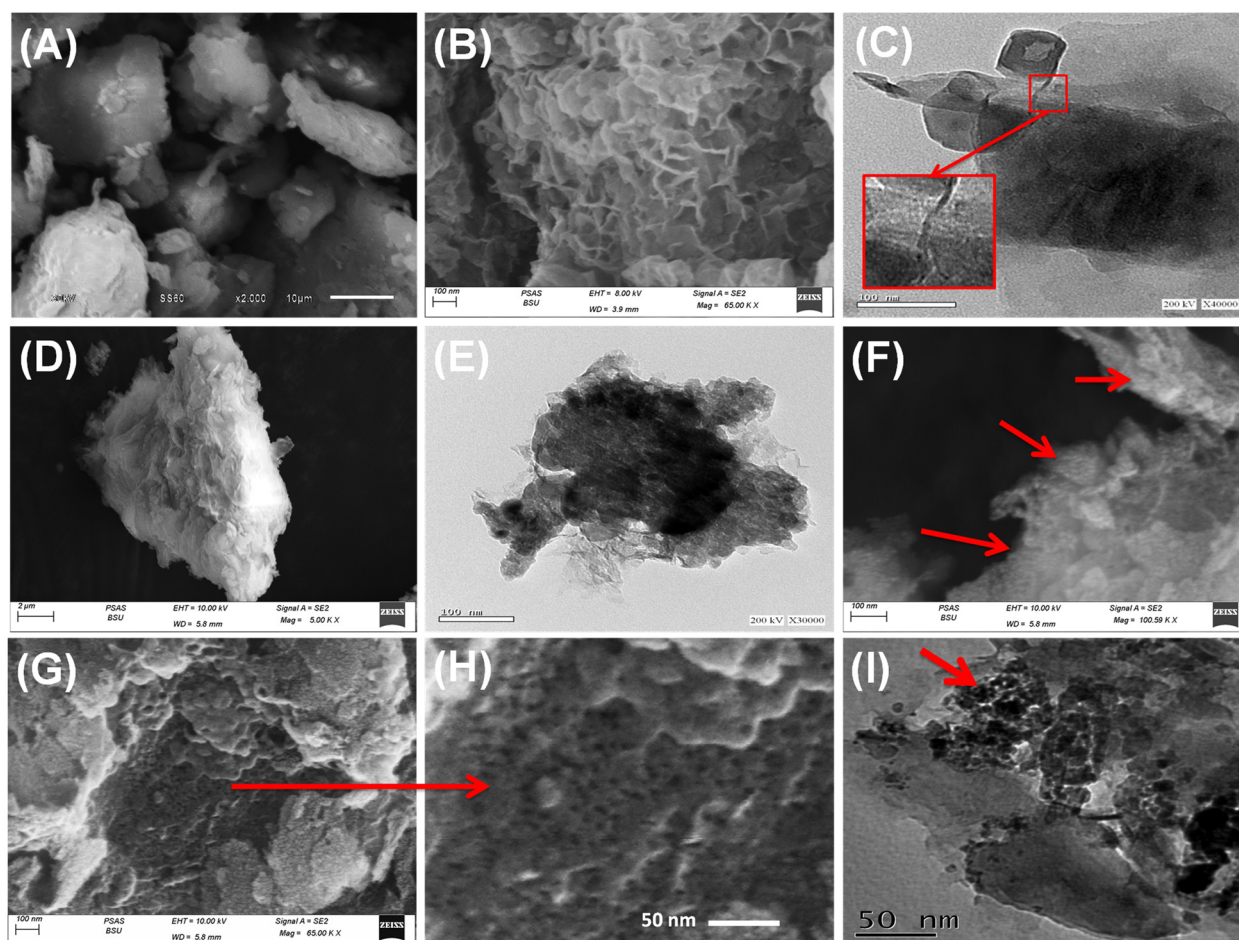

Figure 2. SEM image of raw BEN (**A**,**H**), high-magnification SEM image of BEN surface (**B**), HRTEM images of BEN (**C**), SEM image of CU/BEN (**D**), HRTEM image of CU/BEN (**E**), SEM images of ZN@CU/BEN (**F**–**H**), and HRTEM image of Zn@CU/BEN (**I**) (the red arrow refer to the Zinc oxide particulates).

The morphological impacts caused substantial modifications in the texture of the hybridized structure, particularly in terms of its porosity and surface area. The measured surface areas of BEN (91.2 m^2/g), A.BEN (98.7 m^2/g), Cu/BEN (106.3 m^2/g), and Zn@CU/BEN (156.7 m^2/g) demonstrated significant enhancement in terms of the different modification phases. The significant increase in surface area resulting from the intercalation procedure with the curcumin-derived extracted solutions may be attributed to the expanding and exfoliating effect caused by these elongated organic molecules between the layered units. Additionally, the pillared nanoparticles of zinc metal that grow within the layers of BEN give the structure a very porous feature that significantly increases the surface area. Furthermore, the documented microscopic characteristics of the capped

zinc coating on the exterior of the dispersed BEN sheets are composed of tiny spherical nanoparticles containing large numbers of interstitial nanopores that significantly increase the surface area.

FT-IR spectra were employed to track the chemical functional groups throughout the several transformation operations. The spectrum of the implemented BEN particulates confirmed the presence of the key BEN chemical groups, including coordinated forms of -OH (3400 cm^{-1}) with the structural octahedral ions (AlMg(OH), Al$_2$OH, and AlFe^{3+}(OH)), Si-O (1000 cm^{-1}), interlayer water (1640 cm^{-1}), and Al-O (918 cm^{-1}). The spectral bands ranging from 1000 cm^{-1} to 400 cm^{-1} correspond to the structural bonds of Si-O-Al, Si-O-Mg, Mg-Fe-OH, and Si-O-Si [42,43] (Figure 3A). The spectrum of A.BEN did not show any noticeable appearance of newly formed bands or disappearance of existing bands (Figure 3B). The fundamental impact of the process was demonstrated by the significantly shifted absorption bands, along with the notable enhancement in the magnitude of the distinct bands of the interlayered water and coordinated OH. These changes were a consequence of the hydration influence of the acid washing step (Figure 3B).
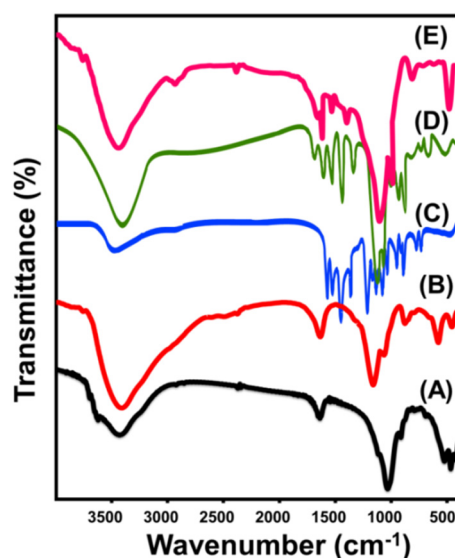

Figure 3. FT–IR spectra of raw BEN (A), activated BEN (B), curcumin (C), CU/BEN (D), and Zn@CU/BEN (E).

The spectrum retrieved for the curcumin powder that was utilized in this study showed the characteristic bands of its principal chemical structure. These include –OH of the phenolic chemicals (3506 cm^{-1}), aromatic C-H (2943–2965 cm^{-1}), C-H of olefin (1432 cm^{-1}), aromatic C-H (1162 and 812 cm^{-1}), cis-CH (716 cm^{-1}), benzoatetrans-CH (963 cm^{-1}), aromatic C-O (1278 cm^{-1}), C=O (1507 cm^{-1}), C-O-C (1023 cm^{-1}), C=C (1626 cm^{-1}), and a benzene ring (1604 cm^{-1}) [37,44]. The CU/BEN spectrum illustrates the effective integration of the inorganic framework of BEN with the organic constituents of the curcumin-derived extract (Figure 3C). The interaction impact is illustrated by the notable displacement of identifying bands representing the crucial chemical groups with respect to the initial materials (Figure 3D). The groups identified in BEN were Si-O (1008 cm^{-1}), Al-O (934 cm^{-1}), Si-O-Si (473.2 cm^{-1}), and Si-O-Al (534 cm^{-1}), while the detectable groups related to curcumin were aromatic C-O (1284 cm^{-1}), benzoatetrans-CH (921 cm^{-1}), C=O (1509 cm^{-1}), olefin C-H (1440 cm^{-1}), and benzene rings (1612 cm^{-1}) (Figure 3D). The established FT-IR spectrum of the synthesized Zn@CU/BEN composite also revealed alterations in the functioning chemical structures (Figure 3E). The organic groups that exist in curcumin-derived phytochemicals, besides the inorganic aluminosilicate-related groups that exist in BEN, were easily detected. The bands revealed significant deviations, indicating the effect of the zinc-pillaring steps (Figure 3E). Furthermore, the weakened bands at 602.7 and 462 cm^{-1} reflected the existence of Zn-O bonds (Figure 3E) [32,33]. This was in good alignment with the -EDX results and validated

the detection of Si and Al representing the inorganic BEN host, C represents the organic compounds of the derived extract, and Zn representing the pillared and coated metal.

2.2. Photocatalytic Degradation Results
2.2.1. Effect of Oxidation Parameters
Effect of pH

Our investigation examined the performance of Zn@CU/BEN as a hybrid catalyst in terms of degrading IBU, with particular emphasis on the influence of pH values ranging from pH 3 to 8. The essential variables were consistently kept at certain values during the experiments. These levels were as follows: dosage of 0.25 g/L, volume of 100 mL, duration of 60 min, concentration of 25 mg/L, and temperature of 20 °C. The described oxidizing measurements demonstrated substantial enhancement when raising the pH towards alkaline conditions, particularly up to a pH of 6. The observed elimination percentage increased from 6.9% at pH 2 to 52.6% at pH 6 (Figure 4A). This tendency may be attributed to the insolubility of IBU within acidic environments and its poor retention characteristics during its molecular state [3,45]. Raising the pH level triggers the hydrophilic characteristics of IBU chemicals, leading to enhanced dissolution and retention of their structure [46]. The binding affinities of Zn@CU/BEN for soluble IBU are negatively affected or may be reversed when the pH is set above 6 (Figure 4A). The observed de-protonation of the existing carboxylate groups within IBU structures may be explained by the repelling interactions between these groups and the dominant negative charges throughout Zn@CU/BEN within alkaline environments [47]. Furthermore, the observed impact caused by elevated pH values on the generation of OH groups—which act as key intermediaries to feed the creation of principal hydroxyl radicals, which constitute the most potent oxidizing species—may also contribute to the improved elimination characteristics with regard to pH [48].
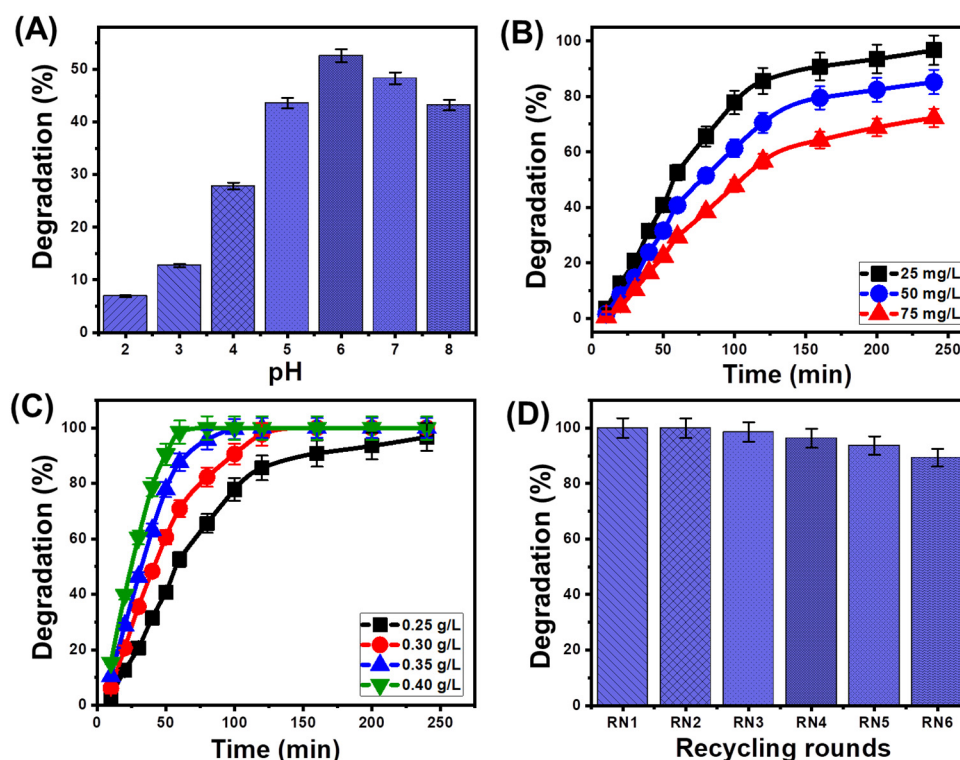

Figure 4. Impact of the testing factors on the oxidation performances of IBU by Zn@CU/BEN including pH (**A**), catalyst dose (**B**), IBU concentration (**C**), and recyclability properties (**D**).

Effects of IBU Concentrations at Different Degradation Durations

The catalytic properties of Zn@CU/BEN were investigated with respect to the period of oxidation (10–240 min) along with the concentrations of IBU (25–75 mg/L). The crucial variables, such as the dosage of 0.25 g/L, overall volume of 100 mL, pH level of 6, and temperature of 20 °C, were unchanged over the duration of the experiments. The Zn@CU/BEN structure exhibited significant oxidative properties throughout the photocatalytic degrading activities of IBU, leading to effective remediation (Figure 4B). The reduction percentages measured for the tested levels of IBU immediately after a period of 240 min were 96.7% (25 mg/L), 85.2% (50 mg/L), and 72.3% (75 mg/L) (Figure 4B). The reduction in the degrading efficiency of Zn@CU/BEN as the content of IBU rises can potentially be credited to the massive formation of thick adsorbed layers of IBU over its surface. The development of extensive coating layers of the adsorbed IBU, in conjunction with the reduced ability of light to penetrate through high IBU levels, ultimately leads to decreased interaction effectiveness between the outer surface of Zn@CU/BEN and incoming light rays [49]. Therefore, the generation of powerful oxidative free radicals is hindered, resulting in an overall decline in the successful completion of the degradation steps. The drop in decomposition rates is particularly notable as the oxidizing time frame is prolonged until reaching a level near the point of equilibrium, around which the degradation system shows a minimal or steady decomposition rate. The observed degradation behavior could potentially be owing to the steady reduction in the quantities of oxidized species generated throughout the IBU disintegration procedures. This decline persists until the complete depletion of these effective species is completed within a particular time frame [48].

Effect of Catalyst Dosage at Different Degradation Durations

The decomposition rates of IBU were evaluated in terms of the implemented dosages of the catalyst within the range of 0.25 g/L to 0.4 g/L of Zn@CU/BEN dosages. This variable is critical for determining the effectiveness of the photocatalytic oxidation reaction at a particular concentration of IBU. The duration of oxidation periods varied between 5 min and 240 min (Figure 4C). The important parameters were maintained at specific values (IBU concentration: 25 mg/L; volume: 100 mL; temperature: 20 °C; pH: 6) throughout testing. Utilizing elevated quantities of Zn@CU/BEN led to a dramatic enhancement in the speed of IBU oxidation, causing a remarkable decrease in the period required to completely degrade the evaluated levels of IBU (Figure 4C). Utilizing Zn@CU/BEN at varying levels (0.3 g/L, 0.35 g/L, and 0.4 g/L) resulted in the complete degradation of 25 mg/L of IBU during particular time periods (160 min, 100 min, and 80 min, respectively) (Figure 4C). The aforementioned behavior has been well-reported in the scientific literature and signifies a notable augmentation in the quantity of operative catalytic sites and the reacting surface area. The previously described investigations revealed that the implementation of Zn@CU/BEN improves the interaction interface involving IBU molecules and its external surface. Furthermore, it results in an increase in the efficiency of the oxidizing agents within the overall system [29,42].

Recyclability of Zn@CU/BEN

Throughout six recycling rounds (RN), the potential of Zn@CU/BEN to be regenerated in numerous cycles of IBU adsorption and degradation was investigated. Following the completion of the tests, the used Zn@CU/BEN portions were filtered and thoroughly rinsed using distilled water for 15 min. Subsequently, they were set aside in a drying furnace at a temperature of 60 °C for a period of 12 h. The potential for recycling of Zn@CU/BEN throughout the oxidation activities of IBU (25 mg/L) was evaluated under identical testing situations corresponding to the oxidizing tests, with a dose of 0.4 g/L and a duration of 100 min at pH 6 (Figure 4D). The findings demonstrated significant sustainability of the Zn@CU/BEN hybrid throughout the oxidization reactions of the IBU medication. The photocatalytic degradation recyclability tests resulted in IBU oxidation levels of 100% (RN1), 100% (RN2), 98.5% (RN3), 96.3% (RN4), 93.7% (RN5), and 89.3% (RN6) (Figure 4D). This

reveals the commercial significance of Zn@CU/BEN, since it could potentially be recycled effectively to eliminate the remaining IBU contaminants in wastewater.

2.2.2. Kinetic and Quantum Yield Studies

The kinetics of the photocatalytic removal reactions of IBU over Zn@CU/BEN were studied using the ideas of first-order (Figure 5A,B) and second-order (Figure 5C,D) models. We adopted regression fitting approaches with the linear formulations in Equations (1) and (2), respectively [22]:

$$\ln \frac{C_o}{C_t} = -\mathrm{k}t \tag{1}$$

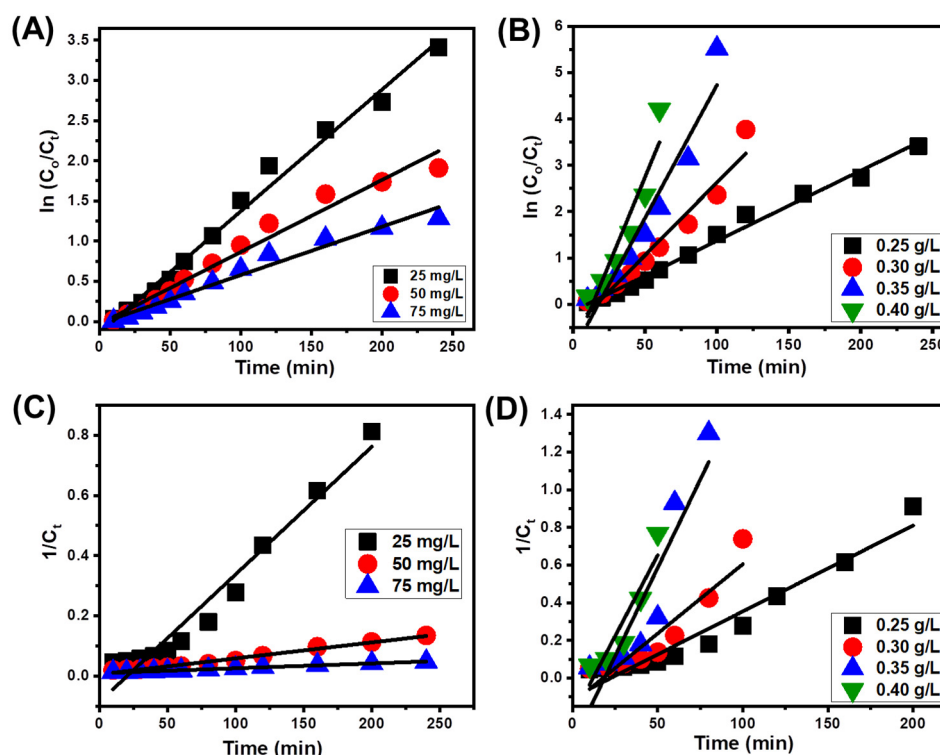$$\frac{1}{C_t} = \frac{1}{C_0} + \mathrm{k}_2 t \tag{2}$$

Figure 5. Fitting of the IBU oxidation results with the first-order kinetic model (**A**,**B**) and second-order kinetic model (**C**,**D**).

The results derived from both of the models revealed agreement with the first-order concept for all Zn@CU/BEN dosages (that varied between 0.25 and 0.4 g/L) and IBU concentrations (that ranged between 25 mg/L and 75 mg/L) (Figure 5; Table 1). The outcomes of this investigation suggest that the performances of the reactions are affected by only the dose of Zn@CU/BEN or by the duration of degradation, rather than both of these factors at the same time. The notable situations that exhibited contemporaneous compliance with both kinetic assumptions indicate the probable collaboration of various degrading processes or the participation of various generated oxidative radicals. The kinetic rate constants estimated for the evaluated models exhibited considerable rise and reduction, respectively, as a consequence of the escalation of Zn@CU/BEN dosages and IBU concentrations (Table 1). The aforementioned outcomes were mostly consistent with the results of experimentation.

Table 1. The kinetic models' fitting criteria and quantum yields.

		First Order		Second Order		Quantum Yield (Φ)
		R^2	K_1	R^2	K_2	
Concentration	25 mg/L	0.986	0.015	0.964	0.0042	7.96×10^{-6}
	50 mg/L	0.981	0.0089	0.974	5.3×10^{-4}	4.72×10^{-6}
	75 mg/L	0.982	0.0060	0.980	1.6×10^{-4}	3.18×10^{-6}
Dosage	0.25 g/L	0.98	0.015	0.96	0.0042	7.96×10^{-6}
	0.3 g/L	0.95	0.031	0.86	0.0073	1.64×10^{-6}
	0.35 g/L	0.93	0.057	0.84	0.0187	3.02×10^{-5}
	0.4 g/L	0.89	0.075	0.87	0.0196	3.98×10^{-5}

The quantum yields (Φ) are crucial metrics for assessing the efficiency of the studied photocatalytic fragmentation process employing Zn@CU/BEN. The theoretical concept of quantum yield throughout the oxidation processes signifies the amount of charge carriers sufficient to accomplish successful decomposition of organic structures by ingested light photons [33,48]. Therefore, the computed values acquired can potentially be employed as indications of the effectiveness displayed by the oxidization systems being studied with respect to the parameters being examined. The determination of apparent quantum yields was performed by calculating the ratio of spent carriers of charges to the total number of photons that entered throughout the experimental environment (Equation (3)) [50,51]. The relevant values of Φ could be calculated by applying Equation (4), which relies on the approximated kinetic rate constants determined according to the first-order model [50–52].

$$\Phi = \frac{Number\ of\ LVOX\ molecules}{Number\ of\ absorbed\ photons} \tag{3}$$

$$\Phi = \frac{K_1}{2.303 \times I_{o,\lambda} \times \varepsilon\lambda \times \ell} \tag{4}$$

The symbols K_1 (S^{-1}), $\varepsilon\lambda$ ($cm^{-1}\ M^{-1}$), I_o, λ (Einstein $I^{-1}\ S^{-1}$), and ℓ (cm) denote the kinetic rate constants, molar absorption, intensity of incident light with a specific wavelength λ, and dimension of the used quartz cell, respectively. The corresponding Φ values for the performed tests utilizing different doses of Zn@CU/BEN and IBU levels are displayed in Table 1. The quantum yields during oxidative reactions displayed augmentation with larger doses of Zn@CU/BEN; however, they indicated a decline with rising levels of IBU. The values that were obtained closely aligned with the results of the experiments and the kinetic significance, demonstrating the increasing influence of the Zn@CU/BEN dosages on the photocatalytic oxidative process of IBU (Table 1).

2.2.3. Synergetic Studies

The impact of the various components, such as the BEN substrate, CU/BEN composite, ZnO, and Zn-pillared BEN (Zn@BEN), on the efficacy of the studied Zn@CU/BEN blend as both an adsorbent and photocatalyst was evaluated using the following parameters:

- BEN, CU/BEN, ZnO, Zn@BEN, and Zn@CU/BEN without light source;
- Visible light source without catalyst;
- Visible light source + catalyst (BEN, CU/BEN, ZnO, Zn@BEN, and Zn@CU/BEN).

The experiments were carried out implementing particular settings for the parameters under consideration, including the catalyst dosage (0.4 g/L), entire volume (100 mL), oxidizing time (120 min), temperature (20 °C), and IBU content (25 mg/L) (Figure 6). In the absence of an illumination source, the incorporation of BEN, CU/BEN, ZnO, Zn@BEN, and Zn@CU/BEN resulted in removal levels of 26.5%, 38.3%, 13.8%, 47.5%, and 63.5% through adsorption, respectively (Figure 6A). This highlights the importance of the blending processes involving those with respect to the adsorption properties of IBU, whether through

the incorporation of extra-functional chemical groups as reactive binding spots or via increasing the surface area.
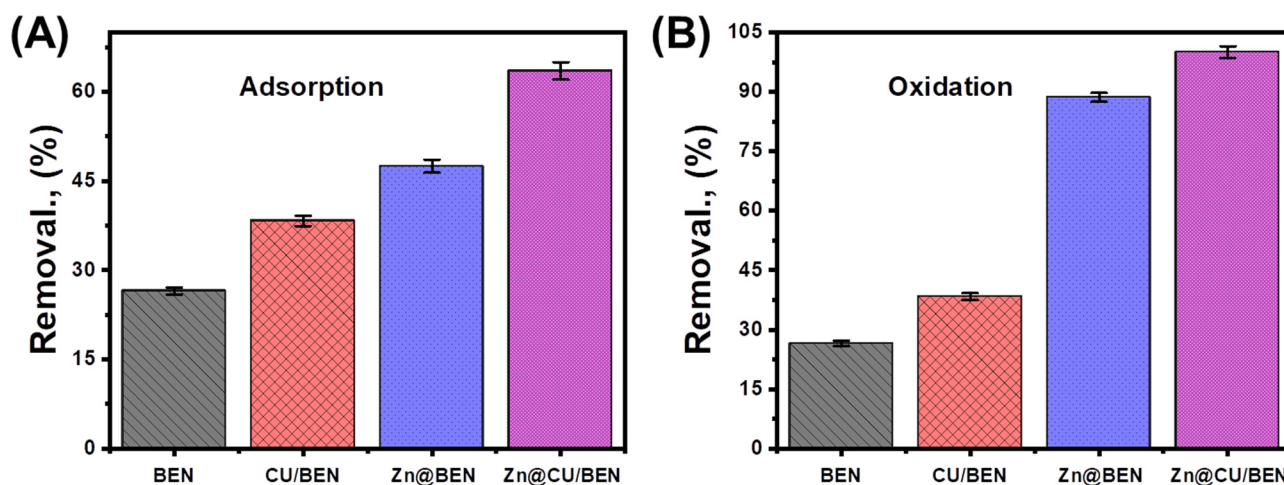

Figure 6. Synergetic effect of the integrated components on the adsorption (**A**) and photocatalytic oxidation (**B**) properties of Zn@CU/BEN.

The IBU compound demonstrated a negligible response to the incident visible light photons, leading to a mere 0.88% reduction in the IBU content. However, employing ZnO, Zn@BEN, and Zn@CU/BEN led to notable catalytic activity and oxidizing impacts on the IBU (Figure 6B), even though the incorporation of BEN and CU/BEN in the context of an illumination source did not demonstrate any significant photocatalytic relevance. The IBU-eliminating percentages obtained with ZnO, Zn@BEN, and Zn@CU/BEN were determined to be 31.7%, 88.6%, and 100%, respectively (Figure 6B). The levels were established after the equilibrium phases of adsorption and desorption. The increase in effectiveness could be attributed to several reasons. Firstly, there was a confirmed increase in the uptake affinity, which is a crucial prerequisite for the effective degradation of pollutants. Furthermore, there was also a rise in the surface area, resulting in an improved interacting interface between the catalytic sites. Furthermore, the consistent dispersion of Zn in the form of pillared nanostructures inside the layers of bentonite promoted the accessibility of the catalytic sites and their interaction with incoming photons. Therefore, it is strongly advised that Zn@CU/BEN should be employed as a cost-effective catalyst when using photocatalytic degradation technology for the remediation of soluble IBU residuals instead of employing the separate constituents BEN, CU/BEN, ZnO, and Zn@BEN.

2.2.4. Mechanism and Pathway
The Affected Oxidizing Species

Determination of the most vital oxidative species that controlled the degradation mechanism of IBU over the Zn@CU/BEN catalyst was performed based on the experimental results of reactive radical entrapping investigations (Figure 7A). Three reagents were employed as entrapping agents to trap the reacting oxidizing species: electron–hole pairs (EDTA-2Na), hydroxyl (Isopropanol (I-P)), and superoxide (1,4-benzoquinone (B-Q)). The tests were conducted with the following adaptations: the Zn@CU/BEN dosage was established at 0.4 g/L, pH at 6, IBU concentration at 25 mg/L, water volume at 100 mL, temperature at 20 °C, duration at 120 min, and volume of trapping chemicals at 1 mmol. The experimental results revealed that the degradation performance or catalytic effectiveness levels of Zn@CU/BEN for IBU dropped to 10.2% (I-P), 90.8% (EDTA-Na), and 65.7% (B-Q) (Figure 7A). Therefore, it seems the oxidative degradation pathway of IBU using Zn@CU/BEN is mainly controlled by the released hydroxyl radicals (OH$^\bullet$) generated through photochemical processes, which are followed by the superoxide species.
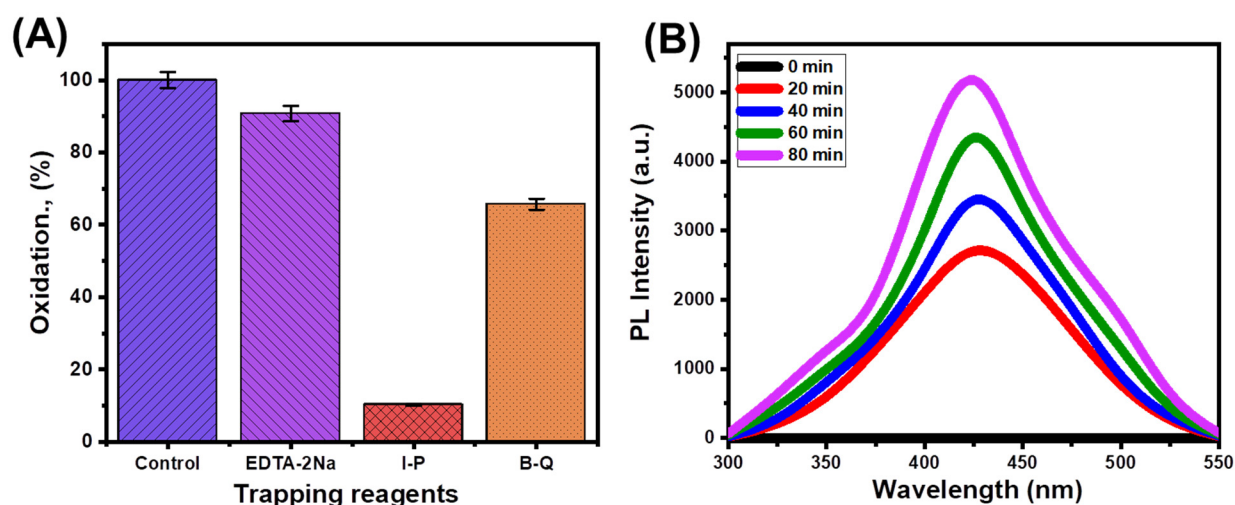
Figure 7. Trapping of the oxidizing radicals during the degradation of IBU by Zn@CU/BEN (**A**) and the change in the measured PL spectra during the oxidation of IBU at different durations (**B**).

Photoluminescence (PL) Detection of the Produced Hydroxyl Radicals

The photoluminescence (PL) method was used to track the presence of OH$^\bullet$, employing the probe molecule methodology (Figure 7B). The test involved mixing 20 mL of terephthalic acid (TA) at a concentration of 5×10^{-4} M with a homogenous mixture containing NaOH at a concentration of 2×10^{-3} M and Zn@CU/BEN particulates weighing 0.5 g. The main result of the chemical reactions involving OH$^\bullet$ and terephthalic acid was the generation of hydroxyterephthalic acid, which displayed a significant photoluminescent signal. The increase in the intensity of the photoluminescent (PL) signal could potentially be ascribed to the simultaneous increase in the release of OH$^\bullet$ provided by the Zn@CU/BEN hybridized form. The photoluminescent (PL) signal was quantified while the oxidation process was underway, by implementing a visible light source positioned at an elevation of about 10 cm distant from the processes. In addition, a 420 nm wavelength cutoff lens was used. The measurement was performed by employing a fluorescence spectrophotometer with a particular wavelength of 425 nm for measurement and an excitation wavelength of 315 nm. The photoluminescence (PL) spectrum of Zn@CU/BEN showed a consistent pattern whenever tested without an illuminating source, suggesting the absence of photocatalytic characteristics. Therefore, it could be stated that no hydroxyl radicals (OH$^\bullet$) were produced during the conditions tested. Whenever the hydroxyterephthalic acid was subjected to the light source, it produced a photoluminescence spectrum that was easily observable (Figure 7B). Moreover, the intensity of the spectrum consistently increased when the duration of the test was prolonged (Figure 7B). The increase in the strength of the photoluminescence (PL) spectrum might be ascribed to a higher amount of OH$^\bullet$ generated by the Zn@CU/BEN components.

The General Oxidation Mechanism

The starting stage in the photocatalytic oxidation of IBU using Zn@CU/BEN as the applied catalyst is the effective uptake of the soluble IBU molecules over the surface of the composite, especially close contact with the active catalytic sites and the released oxidizing radicals. Simultaneously, the excitation of electrons across the outermost layers of pillared Zn metals results in the establishment of electron–hole pairs owing to the significant absorption of the incident radiation [22]. Some of the excited electrons frequently interact with the oxygen ions throughout the degradation circuit, resulting in the emission of superoxide oxidative radicals (O$_2$$^{\bullet-}$) [33]. Furthermore, the occurrence of an electron–hole pair (h$^+$) exerts a disruptive effect on the water molecules, resulting in the emission of hydroxyl oxidative radicals [52]. Afterwards, the oxidative radicals generated, especially the OH$^\bullet$ radicals, react immediately with the soluble IBU compounds, causing oxidation

and degradation of their organic structures. The continuous interactions result in a sequence of oxidizing steps, leading to the establishment of intermediate compounds. Following a period of complete oxidation, these molecules completely transform into carbon dioxide (CO_2) and water (H_2O), as shown by Equations (5)–(11) and Figure 8 [53,54].

$$Zn@CU/BEN + hv \rightarrow Zn@CU/BEN\left(e_{CB}^-, h_{VB}^+\right) \tag{5}$$

$$Zn@CU/BEN\left(e^-\right) + O_2 \rightarrow Zn@CU/BEN + O_2^{\bullet-} \tag{6}$$

$$(Zn@CU/BEN)e^- + IBU \rightarrow (Zn@CU/BEN)e^- + IBU^{+\bullet} \tag{7}$$

$$IBU^{+\bullet} + O_2^{\bullet-} \rightarrow Oxidized\ product \tag{8}$$

$$Zn@CU/BEN\left(h^+\right) + H_2O \rightarrow Zn@CU/BEN + H^+ \uparrow + OH^{\bullet} \tag{9}$$

$$Zn@CU/BEN\left(h^+\right) + IBU \rightarrow Oxidized\ product \tag{10}$$

$$IBU + OH^{\bullet} \rightarrow Oxidized\ product \rightarrow CO_2 + H_2O \tag{11}$$
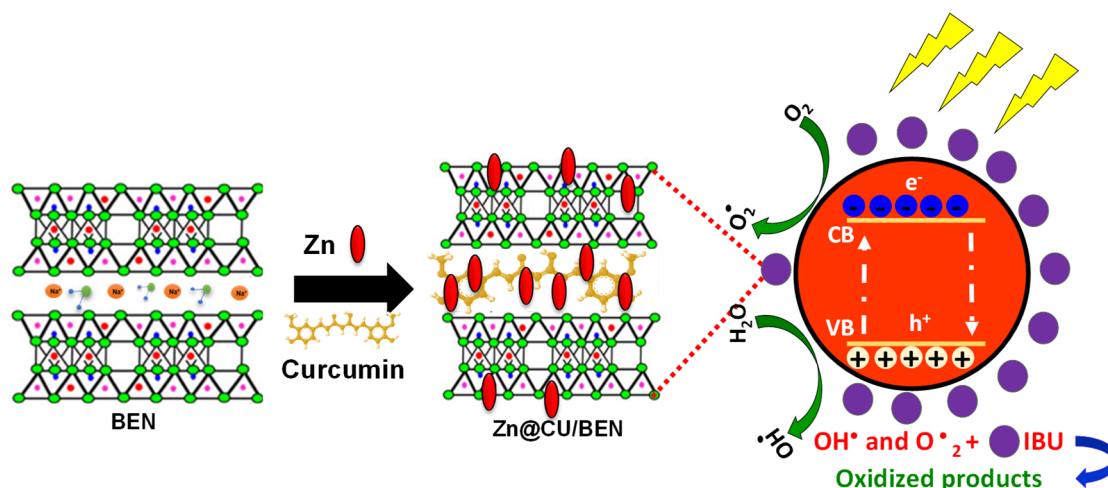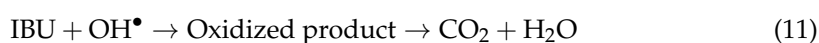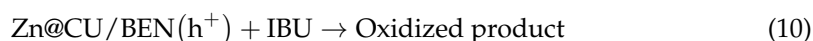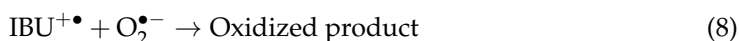

Figure 8. Schematic diagram for the oxidation mechanism of IBU by the Zn@CU/BEN composite.

Mineralization and Oxidation Pathway

TOC Content

The total organic carbon (TOC) concentration in the oxidized IBU-contaminated water samples was monitored to assess the mineralization effectiveness of the degraded IBU compounds and to detect any potential development of intermediate chemicals. The oxidative degradation experiment involved introducing a dose of 0.4 g/L of Zn@CU/BEN. According to the observed curves, there was a significant reduction in the content of total organic carbon (TOC) whenever the oxidation durations increased (Figure 9). Observable disparities existed in the oxidization rates attained for IBU and the TOC elimination percentages established. The observed rates and percentages of TOC elimination in the same situations were significantly lower than the already-established rates and percentages of degradation (Figure 9). The results suggest that the IBU chemicals underwent partial oxidative degradation, which might lead to the formation of secondary intermediate or transitional organic chemicals through modifications or decomposition of the medication's chemical structures. After a period of 160 min, it was established that the photocatalytic treatment, using Zn@CU/BEN as the catalyst, of IBU as a soluble contaminant had led it to become completely degraded, and the TOC content was also removed from the solutions (Figure 9). We can take from this that the Zn@CU/BEN oxidation system of IBU displaced the complete mineralization or decomposition state, producing the final environmentally safe products of CO_2 and H_2O.
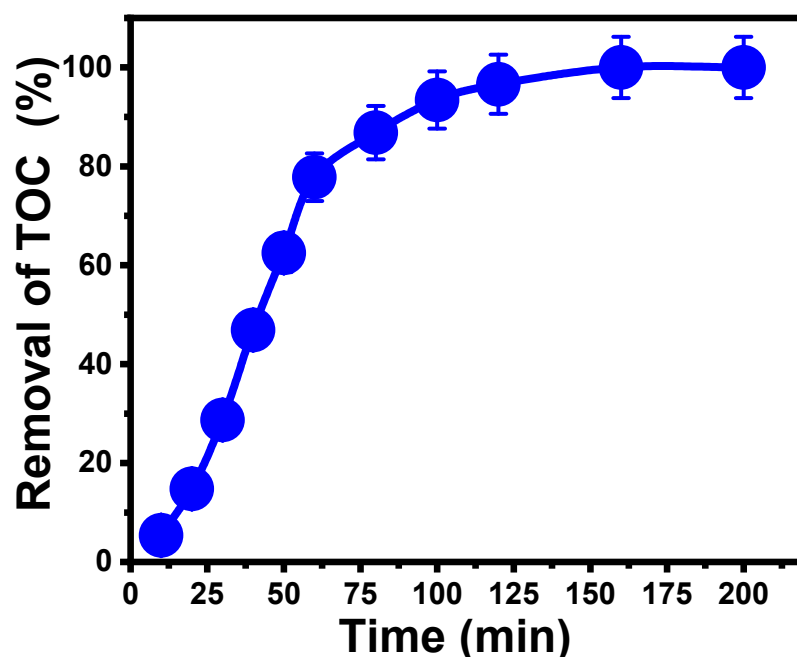
Figure 9. The elimination of the TOC content during the oxidation of IBU by Zn@CU/BEN at different intervals.

Intermediate Compounds and Oxidation Pathway

Several aromatic chemicals were identified in the oxidation of contaminated water samples with IBU, which were treated over the Zn@CU/BEN hybrid material in the presence of visible light (Figure S1, in the Supplementary Materials). These chemicals, which were intermediates or secondary byproducts, included 2-hydroxy-2-(4-isobutyl phenyl) propanoic acid, 1-(4-ethyl phenyl)-2-methyl propan-1-ol, 2-(4-(1-hydroxy-2-methyl propyl) phenyl) propanoic acid, 4-isobutylacetophenone, 2-methyl-butyl benzene, isobutylbenzene, and 4-ethylbenzaldehyde (Figure S1, in the Supplementary Materials). These chemicals or intermediates highlighted the potential oxidation pathways of IBU compounds over the catalytic sites of Zn@CU/BEN. The essential degradation pathway comprises three processes: (1) hydroxylation, (2) decarboxylation/demethylation, and (3) ring-opening phases (Figure 10) [55,56]. The hydroxylation process of the IBU parent chemical structure led to the development of hydroxy-ibuprofen-modified structures, particularly 2-(4-(1-hydroxy-2-methyl propyl) phenyl) propanoic acid and 2-hydroxy-2-(4-isobutyl phenyl) propanoic acid (Figure 10). Subsequently, decarboxylation and demethylation mechanisms occurred, leading to extra oxidation of the intermediates generated. This ultimately resultws in the formation of isobutylbenzene, 1-(4-ethyl phenyl)-2-methyl propan-1-ol, and benzaldehyde, along with various intermediates or secondary chemicals with a small aromatic backbone (Figure 10). The subsequently occurring reaction among the free OH radicals and the ring structures of benzene within the previously generated smaller compounds triggered the formation of different types of carboxylic acids (Figure 10). These carboxylic acids undergo several oxidizing steps, leading to the entire mineralization of IBU into water (H_2O) and carbon dioxide (CO_2) [45].
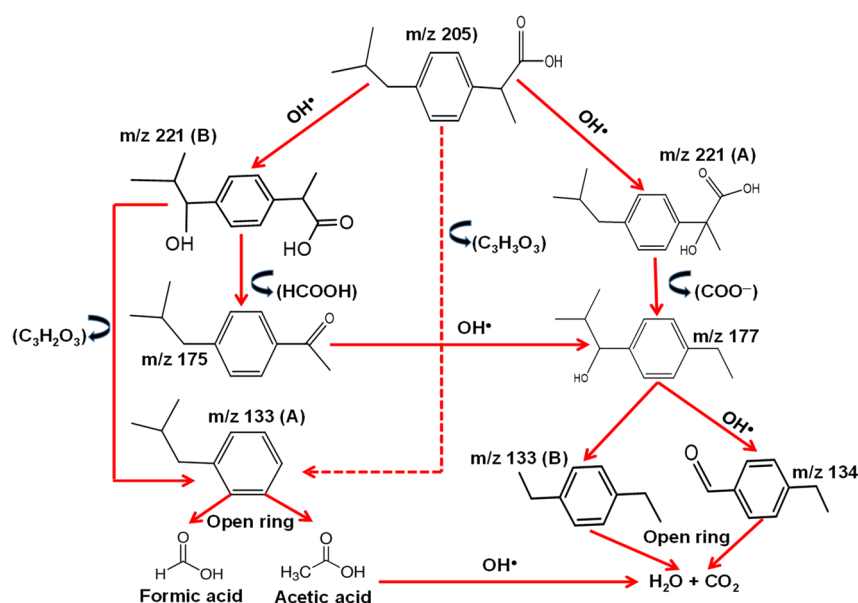
Figure 10. Schematic diagram for the oxidation pathway of IBU by Zn@CU/BEN and the formed intermediates.

2.2.5. Comparison Study

A comparative analysis was conducted to evaluate the efficacy of the synthesized Zn@CU/BEN photocatalyst in eliminating IBU compounds. The analysis considered the oxidizing parameters and the levels of IBU evaluated, and it compared the effectiveness of Zn@CU/BEN with previously studied catalytic structures mentioned in the published literature. The results given demonstrate that the established material has a better level of performance as a photocatalyst for the oxidation of IBU contaminants under visible light. The Zn@CU/BEN catalyst exhibited superior efficacy compared to some synthesized catalysts over brief oxidizing periods, and its application was only necessary in small quantities (Table 2). Consequently, we can surmise that the combination of bentonite and curcumin, along with the incorporation of Zn metal as pillars, allowed us to develop an environmentally friendly blended material with notable enhanced catalytic activities. The resulting material can be implemented effectively for the rapid removal of IBU molecules, which are hazardous medication residues in water.

Table 2. Comparison between the oxidation performance of IBU by Zn@CU/BEN and other investigated catalysts in the literature.

Catalyst	Dosage	Conc.	Light Source	Degradation Performance	Reference
C-N/TiO$_2$	0.50 g/L	20 mg/L	150 W LED lamp	360 min, ca. 98%	[57]
Bi–TiO$_2$	2.00 g/L	10 mg/L	250 W UV lamp	360 min, ca. 89%	[58]
Ag/AgCl@MIL-88A(Fe)	0.40 g/L	10 mg/L	500 W Xe lamp	120 min, ca. 81%	[59]
GQD/AgVO$_3$	0.20 g/L	10 mg/L	350 W Xe lamp	120 min, ca. 91%	[60]
g-C$_3$N$_4$/MIL-68(In)-NH$_2$	0.15 g/L	20 mg/L	300 W Xe lamp	120 min, ca. 93%	[45]
g-C$_3$N$_4$/ZnFeMMO	0.20 g/L	5 mg/L	500 W Xe lamp	240 min, ca. 92%	[61]
Fe$_3$O$_4$@MIL-53(Fe)	0.4 g/L	10 mg/L	500 W Xenon lamp	60 min, ca. 99%	[56]
TiO$_2$-rGO/SOFs	1.00 g/L	5 mg/L	160 W UV lamp	180 min, ca. 81%	[62]
Biochar-ZnAl$_2$O$_4$	1 g/L	20 mg/L	125 W UV lamp	120 min, ca. 100%	[63]
MIL-53(Fe)	0.1 g/L	10 mg/L	500 W Xe lamp	60 min, ca. 99%	[9]
Zn@CU/BEN	0.4 g/L	25 mg/L	400 W metal halide lamp	80 min, ca. 100%	This study

2.2.6. Toxicological Properties

Standardizing in vitro proliferation tests were conducted on two human cell lines: HEK293T, derived from the kidney, and HepG2, derived from the liver (Figure 11). The cell lines were subjected to varying doses (50 μM, 150 μM, and 250 μM) of IBU and its oxidized intermediates in water at varied oxidizing durations individually. After 20 min, the intermediate product of IBU's oxidation had a significant inhibiting impact ($p < 0.05$) on the growth of HEK293T cells (Figure 11A). This detrimental effect was observed throughout all the assessed dosages. Remarkably, the oxidized sample after 20 min, at a concentration of 250 μM, resulted in reduction in the cell viability of HEK293T cells by 22.4% (Figure 11A). This demonstrates a greater inhibiting impact in contrast to the original IBU medication. Furthermore, the sample that underwent oxidation for 60 min had a greater toxic effect, resulting in cell viability of 11.8%. This effect was more pronounced in comparison with IBU at a dose of 250 μM. However, the photodegraded sample after 100 min had little detrimental effect on the proliferation of HEK293T cells as compared to the initial treated samples, resulting in 36% cell viability using the highest dosage (250 μM) (Figure 11A). However, the original form of IBU did not exhibit any noteworthy ($p > 0.05$) inhibiting impact on the HEK293T cell line in any of the doses examined. After 160 min, the treated sample showed no inhibitory impact on the examined cell lines, indicating that the completely mineralized material is safe. This was confirmed by the thorough decomposition of IBU into end products. Several studies have demonstrated the toxic impact of IBU on the human kidney [64,65]. However, in this investigation, IBU did not show any cytotoxic effects, most likely because the quantities utilized were low.
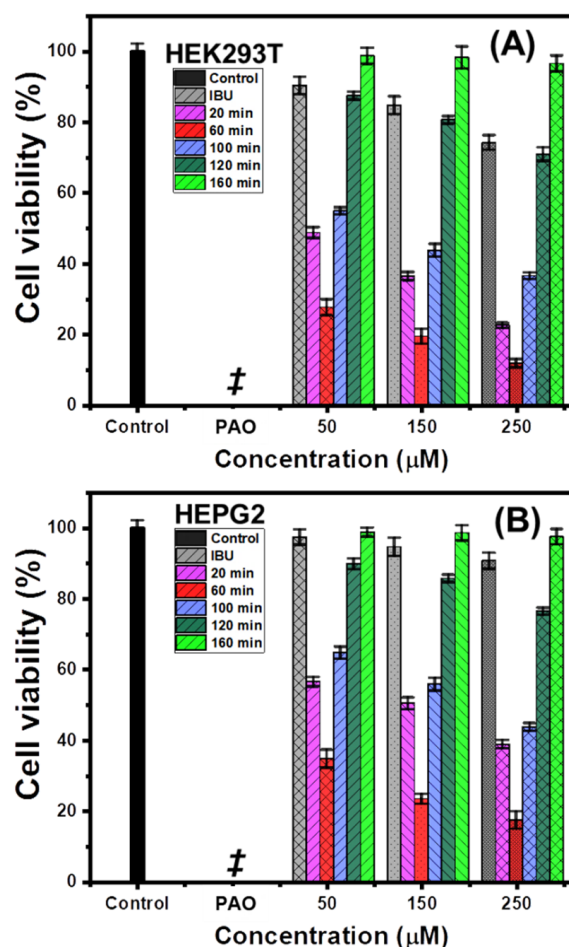

Figure 11. The toxicity effects of the partially and completely oxidized IBU-polluted solutions on HEK293T (**A**) and HEPG2 (**B**) cell lines in the presence of fresh cells as the control and phenylarsine oxide (PAO) as the positive control.

Notably, HEPG2 cells exhibited a comparable effect to the HEK293T cell line (Figure 11B). The growth of HEPG2 cells was inhibited in a dose-dependent way by all the investigated doses collected after 20 min. Remarkably, a dose of 250 µM of the IBU oxidized water sample exhibited a substantially greater inhibition influence on the HEPG2 cell strain in comparison to IBU, resulting in cell viability of 38.8% of the cells (Figure 11B). Moreover, the oxidized sample exhibited a substantial reduction in cell viability at all three doses evaluated after 60 min. Additionally, it had a greater level of inhibition versus IBU at a dosage of 250 µM, resulting in a 17.4% cell viability. The viability of HepG2 cells was not significantly affected by IBU or the completely mineralized IBU-polluted water sample after 160 min, even at the maximum dosage.

In general, the above in vitro experiments established that the photocatalytic degradation byproducts of IBU residuals in the water supply may cause substantial harm to human liver cells and human kidney cells in comparison to the original chemical. Owing to the biological accumulation of such chemicals within human cells and their transfer via food chains, the prolonged consumption of partially oxidized IBU-derived products has the potential to adversely affect liver and kidney functions in humans. Hence, it is necessary to continue the oxidation of IBU using the recommended catalyst for a duration of up to 160 min to be able to accomplish the full mineralization of IBU into a safe end product and prevent the toxic effects of the intermediate compounds.

3. Experimental Work

3.1. Materials and Chemicals

The naturally occurring bentonite sample was collected from a quarry located in the Western Desert of Egypt. The composition of the sample was as follows: 54.82% SiO_2, 2.6% Na_2O, 1.45% TiO_2, 17.56% Al_2O_3, 2.4% CaO, 2.5% MgO, 9.5% Fe_2O_3, and 9.2% LOI (loss on ignition). The hybrid synthesis techniques involved the use of curcumin (>94.99%; its chemical structure is presented in Figure S2, in the Supplementary Materials), sulfuric acid (99%), pure ethanol, zinc nitrate hexahydrate salt (98%), and hydrazine solution (35 wt%), all of which were acquired from Sigma-Aldrich, Cairo, Egypt. For adsorption and oxidation experiments, clinical-grade ibuprofen (98%) was supplied by Sigma-Aldrich, Cairo, Egypt.

3.2. Synthesis of the Catalyst

3.2.1. Acid Activation of Bentonite

To eliminate the existing carbonate and metal impurities, the bentonite fractions were activated using acid. We mixed 10 g of bentonite powdered sample with 100 mL of a dilute (20%) sulfuric acid and mixed them using a magnetic stirrer (650 rpm) over 12 h at 100 °C. Following that, the acid-leached powder was filtered out and then carefully rinsed utilizing distilled water before being dried at room temperature for 48 h (40.3 °C) and stored within specialized containers for subsequent synthesis stages.

3.2.2. Intercalation of Bentonite by Curcumin (CU/BEN)

The bentonite sheets were intercalated using curcumin-extracted organic phytochemicals employing a simple chemical integration process. For this experiment, the curcumin-extracting compounds were obtained by dissolving the curcumin powders (3.7 g) in ethanol (60%) for around 15 min in a sealed vessel at 50 °C and blending the resulting mixture via stirring (1500 rpm). Following this, the resulting mixture was subjected to ultrasound treatment (20 min; 240 W) to increase homogeneity and the yield of the crucial organic phytochemicals. About 50 mL of the resultant extract was homogeneously combined with 4.4 g of BEN as a colloidal solution or suspension in 50 mL of distilled water. To stimulate the diffusion effectiveness of the soluble organic phytochemicals inside the multiple layers of bentonite, the resultant mixture was maintained under rapid stirring (1500 rpm) over 12 h plus ultrasonication over an extra 5 h (240 W). The obtained product after the intercalation (CU/BEN) was subsequently filtrated out of the remaining solution, rinsed carefully for

approximately five runs (10 min), and slowly dried at 50 °C for 12 h before being employed in the following stage (Figure 1).

3.2.3. Synthesis of Zn-Pillared CU/BEN Composite (Zn@CU/BEN)

The synthesis methods commenced by producing green extract solution of curcumin, which functions as a crucial green reagent. This extract was implemented as both a reduction agent and a capping agent. Conversely, the BEN/zinc nitrate combination was developed by thoroughly mixing the CU/BEN portions (4.4 g) with 100 mL of an aqueous solution containing zinc nitrate salt (2.2 g). The blending of the two constituents was carried out over a duration of 10 h by employing a magnetic stirrer operating at a speed of 650 rpm, followed by a further 2 h of sonication utilizing a source with a power output of 240 watts. Subsequently, the curcumin-derived extract (100 mL) was combined with the BEN/zinc nitrate blend while stirring vigorously at a constant rate of 1500 rpm till a noticeable reddish precipitate formed. Following that, rapid introduction of 50 mL of hydrazine was performed to verify the effective transformation of previously generated oxides along with hydroxides towards metallic zinc. The process was extended for a further 24 h with intermittent ultrasound treatments (20 min each) to promote adequate mixing among the reactants and maintain uniform dispersion of the pillared metal as well as the immobilized phytochemicals. Subsequently, the Zn-pillared Cu/BEN composite, in the form of solid particulates (Zn@CU/BEN), was successfully separated via filtering with Whitman filter paper. The filtered product underwent five rounds of washing using distilled water, with each successive washing cycle lasting for 10 min. Subsequently, the rinsed product was dried for 12 h at a temperature of 50 °C.

3.3. Characterization Techniques

The effects of the modifying and combining operations on the crystal structure of BEN were evaluated by analyzing the X-ray diffraction patterns of the different produced materials, achieved by employing a PANalytical-Empyrean X-ray diffractometer (Malvern Panalytical B.V. Co.; Almelo, The Netherlands). The detection span of the diffractometer extended from 5 to 80 degrees. The effects of the modifying chemical processes and the effective insertion of the active ingredient groups of curcumin-related components and ZnO were monitored using the FT-IR spectra. These spectra were obtained using a Fourier transform infrared spectrometer (FTIR-8400S; Shimadzu Co., Kyoto, Japan) over a frequency spectrum of 400 cm^{-1} to 4000 cm^{-1}. A scanning electron microscope (Zeiss Ultra 55; Carl Zeiss AG Co.; Oberkochen, Baden-Württemberg, Germany) was used to examine the exterior morphology, while a transmission electron microscope (JEM-2100, JEOL Ltd. Co.; Tokyo, Japan) was used to analyze the interior characteristics. A surface area analyzer (SA3100, Beckman Coulter Co.; Brea, CA, USA) was used to track the influence of integration processes on the textural qualities and surface area.

3.4. Advanced Oxidation of IBU

The catalytic efficiency of Zn@CU/BEN in oxidizing IBU was assessed after attending to the equilibrium of adsorption as well as desorption inside a Pyrex cylindrical vessel with a diameter equal to 7 cm and an overall length equal to 15 cm. The cell was coupled with a fully embedded visible light bulb positioned 3.5 cm away from the outside surface of the cell. The source of illumination utilized throughout the experiments was a commercially available metal halide bulb with a power output of 400 W and a wavelength of approximately 490 nm. The average incoming illumination intensity was measured to be 18.7 mW/cm^2. Advanced oxidation experiments were conducted using IBU levels of 25, 50, and 75 mg/L, Zn@CU/BEN doses ranging from 0.25 g/L to 0.4 g/L, and oxidizing periods ranging from 10 min to 240 min. The experiments were carried out under constant pH (pH 6), volume (100 mL), and temperature (20 °C) conditions. The overall oxidation performance of IBU was monitored by measuring its concentration within the addressed

solutions. The evaluations were performed three times, and the mean for all three findings exhibited a standard deviation of no more than 4.5%.

The residual IBU levels post adsorption and photocatalytic oxidation experiments, including the secondary byproducts resulting from partial oxidation, were quantified by employing liquid chromatography–mass spectrometry (LC-MS). The LC-MS apparatus was outfitted with a mass analyzer, a 3000 HPLC, and a Thermo Fisher Scientific (Waltham, MA, USA) column. The fluid phase associated with the system consisted of a blend of methanol and water, in addition to formic acid (1%). Throughout the analysis, the eluent was dispensed at a velocity of 0.35 mL/min with an injection capacity of 5 μL, and the column itself was kept at 30 °C. The compounds' mass spectra were measured by employing *m/z* scanning within a 20–400 range, with the nebulizer pressure, temperature, ESI voltage, and nitrogen flow velocity set to 35 psi, 350 °C, 4 kV, and 10 L/min, respectively. The total organic carbon (TOC) contents inside the samples that were oxidized were measured using TOC-VCPH (Shimadzu, Kyoto, Japan) in order to assess the mineralization effectiveness of the oxidation processes.

3.5. Toxicological Properties

The toxicological effects of the oxidized intermediates of IBU on the human body were assessed by examining their impacts on the kidney (HEK293T cell lines) and liver (HepG2 cell lines), using cell lines derived from the American Type Cultural Collection (ATCC). The selected cell lines were grown in DMEMs combined with 10% fetal bovine serum in a humidified atmosphere containing 5% CO_2 at 37 °C. Afterwards, the cells were cultivated and seeded in 96-well plates with a density of 4000 cells per well and incubated overnight. Following that, they were subjected to varied concentrations (250 μM, 150 μM, and 50 μM) of IBU and oxidized IBU-contaminated water within a fresh medium before an extra incubation period of 48 h. Phenylarsine oxide (PAO) served as the positive control, while 0.5% dimethyl sulfoxide (DMSO) served as the negative reference. Following a 48 h incubation period, 20 μL of a 3-(4,5-dimethylthiazol-2-yl)-2,5-diphenyltetrazolium bromide (MTT) reagent with a concentration of 5 mg/mL was introduced into each of the wells. The cells thereafter underwent incubation at a temperature of 37 °C for a duration of 2 h. Following this, the fluids were removed, and 100 μL of DMSO (100%) was injected into each well. Consequently, the absorbance was determined at a wavelength of 570 nm using a microplate reader. The data, described as mean ± standard deviation (%), were reported as the ratio of treated samples to control samples (i.e., IBU or its oxidized products/DMSO). The experiments were conducted in at least three repetitions, with each performed at least three times. The observed data were immediately used to compute the cell viability percentage using Equation (12).

$$\text{Cell viability}(\%) = \frac{\text{Mean OD}}{\text{Control OD}} \times 100 \qquad (12)$$

4. Conclusions

The Zn@CU/BEN composite was synthesized using simple, environmentally friendly approaches for effective catalytic oxidation of IBU into safe end products under visible light. About 25 mg/L of IBU was completely degraded after 80 min using Zn@CU/BEN at 0.4 g/L and pH 6, reflecting higher activity as compared to several study materials. The synergetic influence of BEN and CU/BEN explains the markedly enhanced properties, achieved by inducing the surface area, adsorption capacity, and interactive interface of the catalytic sites of the pillared Zn. The complete elimination of TOC after 160 min demonstrated complete mineralization and the formation of intermediates. The identified intermediates, in addition to the detection of hydroxyl radicals as the effective oxidizing species, validated the degradation of IBU over Zn@CU/BEN through three progressive processes (hydroxylation, decarboxylation/demethylation, and ring opening). The cell viability of kidney (HEK293T) and liver (HEPG2) cell lines after their treatment with the oxidized samples for 160 min revealed high biosafety, with cell viability greater than 97%.

References

1. Ren, Z.; Romar, H.; Varila, T.; Xu, X.; Wang, Z.; Sillanpää, M.; Leiviskä, T. Ibuprofen degradation using a Co-doped carbon matrix derived from peat as a peroxymonosulphate activator. *Environ. Res.* **2020**, *193*, 110564. [CrossRef]

2. Abukhadra, M.R.; Fathallah, W.; El Kashief, F.A.; El-Sherbeeny, A.M.; El-Meligy, M.A.; Awwad, E.M.; Luqman, M. Insight into the antimicrobial and photocatalytic properties of NiO impregnated MCM-48 for effective removal of pathogenic bacteria and toxic levofloxacin residuals. *Microporous Mesoporous Mater.* **2020**, *312*, 110769. [CrossRef]

3. Miranda, M.O.; Cavalcanti, W.E.C.; Barbosa, F.F.; de Sousa, J.A.; da Silva, F.I.; Pergher, S.B.C.; Braga, T.P. Photocatalytic degradation of ibuprofen using titanium oxide: Insights into the mechanism and preferential attack of radicals. *RSC Adv.* **2021**, *11*, 27720–27733. [CrossRef]

4. Lung, I.; Soran, M.L.; Stegarescu, A.; Opris, O.; Gutoiu, S.; Leostean, C.; Lazar, M.D.; Kacso, I.; Silipas, T.D.; Porav, A.S. Evaluation of CNT-COOH/MnO$_2$/Fe$_3$O$_4$ nanocomposite for ibuprofen and paracetamol removal from aqueous solutions. *J. Hazard. Mater* **2021**, *403*, 123528. [CrossRef]

5. Lei, X.; Huang, L.; Liu, K.; Ouyang, L.; Shuai, Q.; Hu, S. Facile one-pot synthesis of hierarchical N-doped porous carbon for efficient ibuprofen removal. *J. Colloid Interface Sci.* **2021**, *604*, 823–831. [CrossRef]

6. Vebber, M.C.; Aguzzoli, C.; Beltrami, L.V.R.; Fetter, G.; Crespo, J.d.S.; Giovanela, M. Self-assembled thin films of PAA/PAH/TiO$_2$ for the photooxidation of ibuprofen. Part II: Characterization, sensitization, kinetics and reutilization. *Chem. Eng. J.* **2018**, *361*, 1487–1496. [CrossRef]

7. Nawaz, M.; Khan, A.A.; Hussain, A.; Jang, J.; Jung, H.Y.; Lee, D.S. Reduced graphene oxide TiO$_2$/sodium alginate 3-dimensional structure aerogel for enhanced photocatalytic degradation of ibuprofen and sulfamethoxazole. *Chemosphere* **2020**, *261*, 127702. [CrossRef]

8. Granatto, C.F.; Grosseli, G.M.; Sakamoto, I.K.; Fadini, P.S.; Varesche, M.B.A. Methanogenic potential of diclofenac and ibuprofen in sanitary sewage using metabolic cosubstrates. *Sci. Total Environ.* **2020**, *742*, 140530. [CrossRef]

9. Yang, S.; Wang, K.; Chen, Q.; Wu, Y. Enhanced photocatalytic hydrogen production of S-scheme TiO$_2$/g-C3N4 heterojunction loaded with single-atom Ni. *J. Mater. Sci. Technol.* **2024**, *175*, 104–114. [CrossRef]

10. Farhadi, N.; Tabatabaie, T.; Ramavandi, B.; Amiri, F. Ibuprofen elimination from water and wastewater using sonication/ultraviolet/hydrogen peroxide/zeolite-titanate photocatalyst system. *Environ. Res.* **2021**, *198*, 111260. [CrossRef]

11. Minella, M.; Bertinetti, S.; Hanna, K.; Minero, C.; Vione, D. Degradation of ibuprofen and phenol with a Fenton-like process triggered by zero-valent iron (ZVI-Fenton). *Environ. Res.* **2019**, *179*, 108750. [CrossRef]

12. Gong, H.; Chu, W.; Huang, Y.; Xu, L.; Chen, M.; Yan, M. Solar photocatalytic degradation of ibuprofen with a magnetic catalyst: Effects of parameters, efficiency in effluent, mechanism and toxicity evolution. *Environ. Pollut.* **2021**, *276*, 116691. [CrossRef]

13. Shanavas, S.; Priyadharsan, A.; Gkanas, E.I.; Acevedo, R.; Anbarasan, P.M. High efficient catalytic degradation of tetracycline and ibuprofen using visible light driven novel Cu/Bi$_2$Ti$_2$O$_7$/rGO nanocomposite: Kinetics, intermediates and mechanism. *J. Ind. Eng. Chem.* **2019**, *72*, 512–528.

14. Chen, C.-H.; Lin, Y.-C.; Peng, Y.-P.; Lin, M.-H. Simultaneous hydrogen production and ibuprofen degradation by green synthesized Cu2O/TNTAs photoanode. *Chemosphere* **2021**, *284*, 131360. [CrossRef]

15. Indira, K.; Shanmugam, S.; Hari, A.; Vasantharaj, S.; Sathiyavimal, S.; Brindhadevi, K.; El Askary, A.; Elfasakhany, A.; Pugazhendhi, A. Photocatalytic degradation of congo red dye using nickel–titanium dioxide nanoflakes synthesized by Mukia madrasapatna leaf extract. *Environ. Res.* **2021**, *202*, 111647. [CrossRef]

16. Gaur, J.; Vikrant, K.; Kim, K.-H.; Kumar, S.; Pal, M.; Badru, R.; Masand, S.; Momoh, J. Photocatalytic degradation of Congo red dye using zinc oxide nanoparticles prepared using Carica papaya leaf extract. *Mater. Today Sustain.* **2023**, *22*, 100339. [CrossRef]

17. Xiang, D.; Lu, S.; Ma, Y.; Zhao, L. Synergistic photocatalysis-fenton reaction of flower-shaped CeO_2/Fe_3O_4 magnetic catalyst for decolorization of high concentration congo red dye. *Colloids Surf. A Physicochem. Eng. Asp.* **2022**, *647*, 129021. [CrossRef]

18. Cui, H.; Yu, J.; Zhu, X.; Cui, Y.; Ji, C.; Zhang, C.; Xue, J.; Jia, X.; Qin, S.; Li, R. Advanced treatment of chicken farm flushing wastewater by integrating Fenton oxidation and algal cultivation process for algal growth and nutrients removal. *J. Environ. Manag.* **2021**, *298*, 113543. [CrossRef]

19. Benisha, R.; Amalanathan, M.; Aravind, M.; Mary, M.S.M.; Ahmad, A.; Tabassum, S.; Al-Qahtani, W.H.; Ahmad, I. Catharanthus roseus leaf extract mediated Ag-MgO nanocatalyst for photocatalytic degradation of Congo red dye and their antibacterial activity. *J. Mol. Struct.* **2022**, *1262*, 133005. [CrossRef]

20. Ghanbari, S.; Fatehizadeh, A.; Khiadani, M.; Taheri, E.; Iqbal, H.M.N. Treatment of synthetic dye containing textile raw wastewater effluent using UV/Chlorine/Br photolysis process followed by activated carbon adsorption. *Environ. Sci. Pollut. Res.* **2022**, *29*, 39400–39409. [CrossRef]

21. Abukhadra, M.R.; Saad, I.; Othman, S.I.; Katowah, D.F.; Ajarem, J.S.; Alqarni, S.A.; Allam, A.A.; Al Zoubi, W.; Ko, Y.G. Characterization of Fe0@ Chitosan/Cellulose structure as effective green adsorbent for methyl Parathion, malachite Green, and levofloxacin Removal: Experimental and theoretical studies. *J. Mol. Liq.* **2022**, *368*, 120730. [CrossRef]

22. Yang, X.; Wang, J.; El-Sherbeeny, A.M.; AlHammadi, A.A.; Park, W.-H.; Abukhadra, M.R. Insight into the adsorption and oxidation activity of a ZnO/piezoelectric quartz core-shell for enhanced decontamination of ibuprofen: Steric, energetic, and oxidation studies. *Chem. Eng. J.* **2022**, *431*, 134312. [CrossRef]

23. Yang, Y.; Chen, X.; Pan, Y.; Song, H.; Zhu, B.; Wu, Y. Two-dimensional ZnS (propylamine) photocatalyst for efficient visible light photocatalytic H2 production. *Catal. Today* **2020**, *374*, 4–11. [CrossRef]

24. Abukhadra, M.R.; AlHammadi, A.A.; Khim, J.S.; Ajarem, J.S.; Allam, A.A.; Shaban, M.S. Enhanced adsorption and visible light photocatalytic removal of 5-Fluorouracil residuals using environmental NiO/geopolymer nanocomposite: Steric, energetic, and oxidation studies. *J. Environ. Chem. Eng.* **2022**, *10*, 108569. [CrossRef]

25. Wang, Z.; Srivastava, V.; Ambat, I.; Safaei, Z.; Sillanpää, M. Degradation of Ibuprofen by UV-LED/catalytic advanced oxidation process. *J. Water Process. Eng.* **2019**, *31*, 100808. [CrossRef]

26. Velsankar, K.; Venkatesan, A.; Muthumari, P.; Suganya, S.; Mohandoss, S.; Sudhahar, S. Green inspired synthesis of ZnO nanoparticles and its characterizations with biofilm, antioxidant, anti-inflammatory, and anti-diabetic activities. *J. Mol. Struct.* **2022**, *1255*, 132420. [CrossRef]

27. Ansari, A.; Ali, A.; Khan, N.; Umar, M.S.; Owais, M. Shamsuzzaman Synthesis of steroidal dihydropyrazole derivatives using green ZnO NPs and evaluation of their anticancer and antioxidant activity. *Steroids* **2022**, *188*, 109113. [CrossRef]

28. Sinha, A.; Sahu, S.K.; Biswas, S.; Mandal, M.; Mandal, V.; Ghorai, T.K. Green approach to synthesize MnxZn1-xO nanocomposite with enhanced photocatalytic, fluorescence and antibacterial activity. *Curr. Res. Green Sustain. Chem.* **2021**, *5*, 100244. [CrossRef]

29. Saad, A.M.; Abukhadra, M.R.; Ahmed, S.A.-K.; Elzanaty, A.M.; Mady, A.H.; Betiha, M.A.; Shim, J.-J.; Rabie, A.M. Photocatalytic degradation of malachite green dye using chitosan supported ZnO and Ce–ZnO nano-flowers under visible light. *J. Environ. Manag.* **2020**, *258*, 110043. [CrossRef]

30. Yusof, N.A.A.; Zain, N.M.; Pauzi, N. Synthesis of ZnO nanoparticles with chitosan as stabilizing agent and their antibacterial properties against Gram-positive and Gram-negative bacteria. *Int. J. Biol. Macromol.* **2018**, *124*, 1132–1136. [CrossRef]

31. Rudayni, H.A.; Rabie, A.M.; Aladwani, M.; Alneghery, L.M.; Abu-Taweel, G.M.; Al Zoubi, W.; Allam, A.A.; Abukhadra, M.R.; Bellucci, S. Biological Activities of *Sargassum* Algae Mediated ZnO and Co Doped ZnO Nanoparticles as Enhanced Antioxidant and Anti-Diabetic Agents. *Molecules* **2023**, *28*, 3692. [CrossRef]

32. Meer, B.; Andleeb, A.; Iqbal, J.; Ashraf, H.; Meer, K.; Ali, J.S.; Drouet, S.; Anjum, S.; Mehmood, A.; Khan, T.; et al. Bio-Assisted Synthesis and Characterization of Zinc Oxide Nanoparticles from Lepidium Sativum and Their Potent Antioxidant, Antibacterial, and Anticancer Activities. *Biomolecules* **2022**, *12*, 855. [CrossRef]

33. Abukhadra, M.R.; AlHammadi, A.A.; Khim, J.S.; Ajarem, J.S.; Allam, A.A. Enhanced decontamination of Levofloxacin residuals from water using recycled glass based a green zinc oxide/mesoporous silica nanocomposite; adsorption and advanced oxidation studies. *J. Clean. Prod.* **2022**, *356*, 131836. [CrossRef]

34. de França, B.M.; Oliveira, S.S.; Souza, L.O.; Mello, T.P.; Santos, A.L.; Forero, J.S.B. Synthesis and photophysical properties of metal complexes of curcumin dyes: Solvatochromism, acidochromism, and photoactivity. *Dye Pigment.* **2022**, *198*, 110011. [CrossRef]

35. Arab, C.; El Kurdi, R.; Patra, D. Efficient removal of Congo red using curcumin conjugated zinc oxide nanoparticles as new adsorbent complex. *Chemosphere* **2021**, *276*, 130158. [CrossRef]

36. Abukhadra, M.R.; Adlii, A.; El-Sherbeeny, A.M.; Soliman, A.T.A.; Elgawad, A.E.E.A. Promoting the decontamination of different types of water pollutants (Cd^{2+}, safranin dye, and phosphate) using a novel structure of exfoliated bentonite admixed with cellulose nanofiber. *J. Environ. Manag.* **2020**, *273*, 111130. [CrossRef]

37. Wasim, M.; Shi, F.; Liu, J.; Zhang, H.; Zhu, K.; Tian, Z. Synthesis and characterization of curcumin/MMT-clay-treated bacterial cellulose as an antistatic and ultraviolet-resistive bioscaffold. *J. Polym. Res.* **2022**, *29*, 423. [CrossRef]

38. Arabmofrad, S.; Jafari, S.M.; Lazzara, G.; Ziaiifar, A.M.; Shahiri Tabarestani, H.; Bahlakeh, G.; Cavallaro, G.; Calvino, M.M.; Nasiri Sarvi, M. Preparation and characterization of surface-modified montmorillonite by cationic surfactants for adsorption purposes. *J. Therm. Anal. Calorim.* **2023**, *148*, 13803–13814. [CrossRef]

39. Tong, L.; Liang, T.; Tian, Y.; Zhang, Q.; Pan, Y. Research progress on treatment of mine wastewater by bentonite composite. *Arab. J. Geosci.* **2022**, *15*, 1–23. [CrossRef]

40. Koksal, E.; Afsin, B.; Tabak, A.; Caglar, B. Butylamine-resadiye bentonite composite characterization. *Spectrosc. Lett.* **2020**, *53*, 745–750. [CrossRef]

41. Nagahashi, E.; Ogata, F.; Saenjum, C.; Nakamura, T.; Kawasaki, N. Preparation and Characterization of Acid-Activated Bentonite with Binary Acid Solution and Its Use in Decreasing Electrical Conductivity of Tap Water. *Minerals* **2021**, *11*, 815. [CrossRef]

42. Salam, M.A.; Mokhtar, M.; Albukhari, S.M.; Baamer, D.F.; Palmisano, L.; Jaremko, M.; Abukhadra, M.R. Synthesis and Characterization of Green ZnO@ polynaniline/Bentonite Tripartite Structure (G. Zn@ PN/BE) as Adsorbent for As (V) Ions: Integration, Steric, and Energetic Properties. *Polymers* **2022**, *14*, 2329. [CrossRef]

43. Dardir, F.M.; Mohamed, A.S.; Abukhadra, M.R.; Ahmed, E.A.; Soliman, M.F. Cosmetic and pharmaceutical qualifications of Egyptian bentonite and its suitability as drug carrier for Praziquantel drug. *Eur. J. Pharm. Sci.* **2018**, *115*, 320–329. [CrossRef]

44. Deng, J.; Wang, J.; Hu, H.; Hong, J.; Yang, L.; Zhou, H.; Xu, D. Application of mesoporous calcium silicate nanoparticles as a potential SD carrier to improve the solubility of curcumin. *J. Dispers. Sci. Technol.* **2022**, *44*, 2258–2266. [CrossRef]

45. Cao, W.; Yuan, Y.; Yang, C.; Wu, S.; Cheng, J. In-situ fabrication of g-C3N4/MIL-68 (In)-NH2 heterojunction composites with enhanced visible-light photocatalytic activity for degradation of ibuprofen. *Chem. Eng. Trans.* **2020**, *391*, 123608. [CrossRef]

46. Abukhadra, M.R.; Refay, N.M.; Nadeem, A.; El-Sherbeeny, A.M.; Ibrahim, K.E. Insight into the role of integrated carbohydrate polymers (starch, chitosan, and β-cyclodextrin) with mesoporous silica as carriers for ibuprofen drug; equilibrium and pharmacokinetic properties. *Int. J. Biol.* **2020**, *156*, 537–547. [CrossRef]

47. Martín, J.; Orta, M.d.M.; Medina-Carrasco, S.; Santos, J.L.; Aparicio, I.; Alonso, E. Evaluation of a modified mica and montmorillonite for the adsorption of ibuprofen from aqueous media. *Appl. Clay Sci.* **2019**, *171*, 29–37. [CrossRef]

48. Wang, C.; Sun, R.; Huang, R.; Cao, Y. A novel strategy for enhancing heterogeneous Fenton degradation of dye wastewater using natural pyrite: Kinetics and mechanism. *Chemosphere* **2021**, *272*, 129883. [CrossRef]

49. Abdullah, R.R.; Shabeed, K.M.; Alzubaydi, A.B.; Alsalhy, Q.F. Novel photocatalytic polyether sulphone ultrafiltration (UF) membrane reinforced with oxygen-deficient Tungsten Oxide (WO2.89) for Congo red dye removal. *Chem. Eng. Res. Des.* **2021**, *177*, 526–540. [CrossRef]

50. Huda, A.; Ichwani, R.; Handoko, C.T.; Bustan, M.D.; Yudono, B.; Gulo, F. Comparative photocatalytic performances towards acid yellow 17 (AY17) and direct blue 71 (DB71) degradation using Sn3O4 flower-like structure. *J. Phys. Conf. Ser.* **2019**, *1282*, 012097. [CrossRef]

51. Shemy, M.H.; Othman, S.I.; Alfassam, H.E.; Al-Waili, M.A.; Alqhtani, H.A.; Allam, A.A.; Abukhadra, M.R. Synthesis of Green Magnetite/Carbonized Coffee Composite from Natural Pyrite for Effective Decontamination of Congo Red Dye: Steric, Synergetic, Oxidation, and Ecotoxicity Studies. *Catalysts* **2023**, *13*, 264. [CrossRef]

52. Shams-Ghahfarokhi, Z.; Nezamzadeh-Ejhieh, A. As-synthesized ZSM-5 zeolite as a suitable support for increasing the photoactivity of semiconductors in a typical photodegradation process. *Mater. Sci. Semicond. Process.* **2015**, *39*, 265–275. [CrossRef]

53. Adly, E.R.; Shaban, M.S.; El-Sherbeeny, A.M.; Al Zoubi, W.; Abukhadra, M.R. Enhanced Congo Red Adsorption and Photo-Fenton Oxidation over an Iron-Impeded Geopolymer from Ferruginous Kaolinite: Steric, Energetic, Oxidation, and Synergetic Studies. *ACS Omega* **2022**, *7*, 31218–31232. [CrossRef] [PubMed]

54. Sun, Q.; Hu, X.; Zheng, S.; Zhang, J.; Sheng, J. Effect of calcination on structure and photocatalytic property of N-TiO2/g-C3N4@diatomite hybrid photocatalyst for improving reduction of Cr(VI). *Environ. Pollut.* **2019**, *245*, 53–62. [CrossRef]

55. Liu, S.H.; Tang, W.T. Photodecomposition of ibuprofen over g-C3N4/Bi2WO6/rGO heterostructured composites under visible/solar light. *Sci. Total Environ.* **2020**, *731*, 139172. [CrossRef]

56. Liu, N.; Wang, J.; Wu, J.; Li, Z.; Huang, W.; Zheng, Y.; Lei, J.; Zhang, X.; Tang, L. Magnetic Fe3O4@MIL-53(Fe) nanocomposites derived from MIL-53(Fe) for the photocatalytic degradation of ibuprofen under visible light irradiation. *Mater. Res. Bull.* **2020**, *132*, 111000. [CrossRef]

57. Yang, Y.; Ok, Y.S.; Kim, K.-H.; Kwon, E.E.; Tsang, Y.F. Occurrences and removal of pharmaceuticals and personal care products (PPCPs) in drinking water and water/sewage treatment plants: A review. *Sci. Total Environ.* **2017**, *596–597*, 303–320. [CrossRef]

58. Archer, E.; Petrie, B.; Kasprzyk-Hordern, B.; Wolfaardt, G.M. The fate of pharmaceuticals and personal care products (PPCPs), endocrine disrupting contaminants (EDCs), metabolites and illicit drugs in a WWTW and environmental waters. *Chemosphere* **2017**, *174*, 437–446. [CrossRef]

59. Gogoi, A.; Mazumder, P.; Tyagi, V.K.; Tushara Chaminda, G.G.; An, A.K.; Kumar, M. Occurrence and fate of emerging contaminants in water environment: A review. *Groundw. Sustain. Dev.* **2018**, *6*, 169–180. [CrossRef]

60. Liu, J.-L.; Wong, M.-H. Pharmaceuticals and personal care products (PPCPs): A review on environmental contamination in China. *Environ. Int.* **2013**, *59*, 208–224. [CrossRef]

61. Rivera-Utrilla, J.; Sánchez-Polo, M.; Ferro-García, M.Á.; Prados-Joya, G.; Ocampo-Perez, R. Pharmaceuticals as emerging contaminants and their removal from water. A review. *Chemosphere* **2013**, *93*, 1268–1287. [CrossRef] [PubMed]

62. Petrie, B.; Barden, R.; Kasprzyk-Hordern, B. A review on emerging contaminants in wastewaters and the environment: Current knowledge, understudied areas and recommendations for future monitoring. *Water Res.* **2015**, *72*, 3–27. [CrossRef]

63. Siara, S.; Elvis, C.; Harishkumar, R.; Chellam, P.V. ZnAl$_2$O$_4$ supported on lychee-biochar applied to ibuprofen photodegradation. *Mater. Res. Bull.* **2021**, *145*, 111530. [CrossRef]

64. Balestracci, A.; Ezquer, M.; Elmo, M.E.; Molini, A.; Thorel, C.; Torrents, M.; Toledo, I. Ibuprofen-associated acute kidney injury in dehydrated children with acute gastroenteritis. *Pediatr. Nephrol.* **2015**, *30*, 1873–1878. [CrossRef] [PubMed]

65. Modig, S.; Elmståhl, S. Kidney function and use of nonsteroidal anti-inflammatory drugs among elderly people: A cross-sectional study on potential hazards for an at risk population. *Pharm. Weekbl.* **2018**, *40*, 870–877. [CrossRef] [PubMed]